Journal of Aerosol Science 165 (2022) 106039

Contents lists available at ScienceDirect

Journal of Aerosol Science

journal homepage: www.elsevier.com/locate/jaerosci

Minimizing the coincidence error in particle size spectrometers with digital signal processing techniques

Lukas Oeser [a,*], Nakul Samala [b], Lars Hillemann [b], Andreas Rudolph [b], Jens Lienig [c]

[a] Technische Universität Dresden, Institute of Electromechanical and Electronic Design, Topas GmbH, Gasanstaltstraße 47, D-01237, Dresden, Germany
[b] Nakul Samala, Topas GmbH, Gasanstaltstraße 47, D-01237, Dresden, Germany
[c] Technische Universität Dresden, Institute of Electromechanical and Electronic Design, D-01062, Dresden, Germany

ARTICLE INFO

Keywords:
Particle size spectrometer
Coincidence error
Peak detection
Wavelet analysis
Dead time

ABSTRACT

Aerosol quantification is highly coveted for many applications ranging from quality monitoring to healthcare. Optical particle size spectrometers are one of the popular measurement devices used in aerosol characterization, which provide information about the size distribution and concentration of the particles. One drawback of this method is that the spectrometers are limited to applications with relatively low concentrations. At high concentrations, the number concentration is underestimated, while the size distribution is shifted towards larger particles. This phenomenon is commonly referred as coincidence error. However, the counting efficiency, above the lower detection limit, depends i. a. on the detector dead time. In order to minimize the probability of coincidence events, the dead time of the detector has to be as small as possible. The contribution of this work is to minimize the coincidence error by purposefully reducing the detector dead time. Therefore, various digital signal processing methods, to minimize dead time, are investigated and experimentally verified. Wavelet and derivative-based peak detection algorithms were found to be able to separate even strongly overlapping scattered light pulses from each other. The results show that the detector dead time can be reduced by 65% with digital signal processing techniques. Allowing the quantification of aerosols with more than 2.9 times the maximum concentration of current optical aerosol spectrometers, without increasing the coincidence error.

1. Introduction

Optical particle size spectrometers are used to measure the number concentration and the size distribution of aerosols in the size range from approximately 70 nm up to 25 µm (VDI 3867 Blatt 4, 2011). The measurement principle is based on the analysis of the scattered light. An aerosol is passed through an illuminated measuring volume. If a particle is located in the measuring volume, the light is scattered in different spatial directions depending on its size, shape, orientation and refractive index. For spherical particles the interaction with light can be described by the Mie theory (Mie, 1908). The intensity of the light scattered from the particles can be measured using photodetectors (e. g. photodiode, avalanche photodiode, silicon photomultiplier, photomultiplier tube) and is converted into an electrical signal. The intensity of the scattered light pulses contains information about the particle size. Finally, the

---

* Corresponding author.
E-mail address: loeser@topas-gmbh.de (L. Oeser).

https://doi.org/10.1016/j.jaerosci.2022.106039
Received 9 February 2022; Received in revised form 31 May 2022; Accepted 10 June 2022

pulses can be counted and assigned into different size classes. However, the method is limited by coincidence errors. At high concentrations, the probability for more than one particle in the measuring volume at a time increases. This leads to overlapping pulses in the output signal, which reduces the counting efficiency (ratio between the number of particles counted and the actual number of particles) of the spectrometer. As a result, the number concentration is underestimated, while the particle size tends to be overestimated (Raasch & Umhauer, 1984). Practically, the effect of coincidence limits the application of particle size spectrometers to number concentrations below 10^5 cm^{-3} (VDI 3867 Blatt 4, 2011). Indeed there are several approaches to minimize the coincidence error. In general, a small measuring volume decreases the probability of two particles in the measuring volume. According to the model of the Gaussian beam, light cannot be focused infinitely. With modern line laser modules, measuring volume heights of about 20 μm can be achieved. The other dimensions are usually given by the aerosol stream. Note that the measuring volume can also be defined by optically setting a well-defined volume inside the aerosol stream. This may cause a border zone error. There are some techniques that use a special geometry for the measuring volume to avoid this (VDI 3867 Blatt 4, 2011; Moelter & Munzinger, 1998). However, this work is addressed to particle size spectrometers with a measuring volume, delimited by one or more laser diodes and the aerodynamic focusing let the entire aerosol stream pass through the measuring volume.

To the best of our knowledge, the analysis of the light impulses, scattered from the particles, is typically performed by threshold-based algorithms. Those can be implemented either with an analog circuit, consisting of a comparator in combination with a peak detector or by adopting digital signal processing (Sachweh, 1991). If the detector signal rises above a predefined threshold, this event is considered and counted as a peak. The disadvantage of this approach is that the detector signal has to fall below the threshold before the next particle can be counted. This leads to a large detector dead time (typically >10 μs) causing unnecessary high coincidence errors. The potential of digital signal processing is not fully utilized with this simple detection algorithm. This work exhibits how advanced algorithms can be used to reduce the detector dead time by evaluating the shape of the particle pulses.

Particle size spectrometers, usually work at a constant sample flow rate that ensures all particles move through the measuring volume at approximately same velocity (VDI 3867 Blatt 4, 2011). As the intensity of a Gaussian beam can be described as a normal distribution, every particle generates a Gaussian peak on the detector signal. In case of coincidence, the peaks overlap each other. The high detector apertures allow the assumption of an additive correlation between the intensity of each particle. The detector signal can be described by the following equation:

$$U(t) = U_0 + U_{noise}(t) + \sum_{j=0}^{M} A_j \cdot e^{-\frac{\left(t-t_j\right)^2}{2\cdot\sigma_j^2}} \qquad \text{Equation 1}$$

The signal offset U_0 is caused by the dark current of the photodetector. Although it changes with temperature, this value is assumed to be constant over time. The noise of the photodetector and the electronics is modeled with the term $U_{noise}(t)$. Finally, the last term describes the peaks from the particles measured at the time t_j. The amplitude A_j depends on the particle size, while the parameter σ_j defines the peak width.

From the perspective of signal processing, a coincidence event occurs when there are simultaneously two or more particles in the measuring volume, and the distance between the particles becomes so small that the detection system cannot sperate the peaks anymore. This can be illustrated with the model of dead time (Fig. 1).

The equation for the counting efficiency (ratio of counted particles $M_{counted}$ to actual present particles M_{actual}) of the aerosol spectrometer can be derived from the Poisson statistics (Equation (2)) (VDI 3867 Blatt 4, 2011). For a given aerosol concentration c and sample flow rate $\dot{V}$, the counting efficiency η can be increased by minimizing the detector dead time T_d. Thus, a good peak detection algorithm for an aerosol spectrometer must be able to detect overlapping Gaussian peaks on a noisy baseline.

$$\eta = \frac{M_{counted}}{M_{actual}} = e^{-c\cdot\dot{V}\cdot T_d} \qquad \text{Equation 2}$$

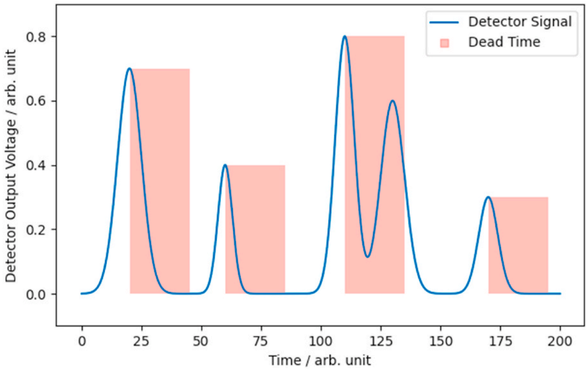

Fig. 1. Simulated detector signal of a particle spectrometer. The fourth particle pulse is not counted, because it is inside the dead time (red zones). (For interpretation of the references to colour in this figure legend, the reader is referred to the Web version of this article.)

The algorithms, used for peak detection, are usually threshold-based, i. e., the detector signal is compared with a threshold. If the detector signal rises above the threshold, the event is counted as a pulse. The threshold does not have to be a fixed value. For example, if the detector dark current varies due to a temperature change, the baseline signal will be shifted. Therefore, the threshold should be set depending on the baseline level. The z-scores algorithm additionally calculates the standard deviation of the signal in order to measure the noise level (Brakel, 2014). This way, the threshold can be set to a confidence interval which depends on the signal quality.

In general, the robustness of threshold-based algorithms can be increased by measuring how long the signal is above the threshold (Sachweh, 1991). False peaks can be excluded using a lower and upper time limit. However, threshold-based detection algorithms have an obvious disadvantage. To detect small particles, it is necessary to keep the threshold as close as possible to the baseline. If one peak is detected the signal needs to fall below the threshold, before the next peak can be detected. Due to the Gaussian peak shape, this can usually take longer than 10 μs. This effect becomes noticeable after a large particle (e. g. > 1 μm) when the peak amplitude is high, especially when the size is close to the upper detection limit with respect to size. According to Mie-theory, the intensity of the light scattered from a particle is proportional to the sixth power of the diameter (For $D_p \ll \lambda$) (VDI 3867 Blatt 4, 2011; Mie, 1908). Thus, the measurement signal has to be evaluated over a wide dynamic range. The challenge of detecting overlapping Gaussian peaks is not new. Hence, a variety of different approaches could be found in the literature. The automated evaluation of spectroscopic measurement methods such as, gamma-ray spectroscopy (Li et al., 2019), mass spectroscopy (Abramovitch, 2020; Du et al., 2006), Raman-spectroscopy (Liu et al., 2018), chromatography (Tong et al., 2016; Viv ó -Truyols et al., 2005; Zhao et al., 2019), and capillary electrophoresis (Jiao et al., 2008; Wee et al., 2008), does often require the detection of overlapping Gaussian peaks in a noisy spectrum. The significant difference is that all of the methods are used for the offline analysis of the spectra. Accordingly, the algorithms have abundant time for signal processing. The requirements for the analysis of the detector signal in aerosol spectrometers are quite different, the processing has to be done in real-time on a continuous measurement signal. Nevertheless, some of the approaches can still be used for analyzing the particle pulses.

From a mathematical point of view, the detector signal can be analyzed by differential calculus. The maxima of the peaks can be found by looking for zeros in the first derivative. If the distance between the peaks decreases, the analysis of the first derivate is not sufficient, because the overlapped peak does not provide a local maxima anymore. In this case, it is necessary to analyze the negative zones of the second derivative, as shown in the work of Vivó-Truyols (Viv ó -Truyols et al., 2005). In theory, it is even possible to process the third derivative. However, the calculation of derivatives, which is usually done with the difference quotient, increases the signal noise (Abramovitch, 2020; Jiao et al., 2008; Li et al., 2019; Viv ó -Truyols et al., 2005). The third derivative should be used with caution, and only for signals with sufficient signal quality. Low pass filters can only partially counteract this, since they affect the signal shape. It might be better to use the Savitzky-Golay filter to obtain the derivatives, as this filter keeps the original pulse form (Savitzky & Golay, 1964). The Savitzky-Golay filter requires the parameters, polynomial degree and window size. Vivó-Truyols et al. (2005) presents a method to obtain the optimal parameters by Durbin-Watson statistics (Viv ó -Truyols et al., 2005).

Another method to detect overlapped Gaussian peaks is to utilize the wavelet transformation (Du et al., 2006; Liu et al., 2018; Wee et al., 2008; Zhao et al., 2019). The measured signal $x(t)$ is convoluted with kernel $\psi(a, b)$:

$$W(a,\ b) = \frac{1}{\sqrt{a}} \cdot \int_{-\infty}^{\infty} \psi\left(\frac{t-b}{a}\right) \cdot x(t) \cdot dt \qquad \text{Equation 3}$$

The wavelet-transformed signal is a measure of similarity between the original signal and the kernel function. So, in the case of an aerosol spectrometer the particle pulses are amplified, while the signal noise is suppressed. Depending on the kernel function, more or less overlapped peaks are detected. Practically, the Ricker wavelet (also known as the Mexican hat wavelet) is often used. It has a single major peak and the form of the second derivative of a Gaussian function. The translation parameter a defines the shift of the kernel, while the scaling parameter b defines the width of the kernel. The kernel width has to match with the particle pulses in the detector signal. If the scaling factor is too high, adjacent pulses cannot be detected anymore. A small scaling factor, on the other hand, has an improved peak resolution but is more sensitive to noise. The peak detection algorithms presented in (Liu et al., 2018) and (Zhao et al., 2019) use multiple scaling factors for pulse shape analysis. The wavelet-transformation can be seen as a map with height profiles. Here, the peaks are represented as ridgelines. Due to the constant pulse width, caused by the regulated sample flow rate, the use of multiple scaling factors is not necessary for aerosol spectrometers.

In the case of an aerosol spectrometer, the wavelet transformation has to be calculated for a continuous, time discrete signal. As the value of the kernel approaches zero for minus infinity and infinity, the limits of integration can be set to a rational value. Thus, the calculation of the wavelet transformed signal $w[n]$, at position n, can be simplified for a single scaling factor and a time discrete input signal $x[n]$:

$$w[n] = \sum_{i=0}^{N} \varphi[i] \cdot x[n-i] \qquad \text{Equation 4}$$

Practically, the calculation of Equation (4) can be easily done with a Finite Impulse Response (FIR) filter of the order N, with filter coefficients $\varphi[i]$. For further information on the wavelet transformation and the structure of a FIR filter, refer to Appendix A.

2. Material and methods

2.1. Implemented algorithms

The counting efficiency of four different peak detection algorithms (i. e., Fixed Threshold, Z-Scores, Vivó-Truyols, Wavelet, Wavelet-Derivate) was compared to that of a recent aerosol spectrometer (LAP 323, Topas GmbH, Dresden, Germany). To ensure real-time capability, the algorithms were implemented on a Field Programmable Gate Array (FPGA). A short overview of the working principle of the different algorithms is provided in the following.

Fixed Threshold: The detector signal is compared with a predefined threshold value. If the signal is above this value for a certain amount of time, the event is counted as a peak. The counting efficiency of this algorithm is expected to match with the analog signal processing of the aerosol spectrometer.

Z-Scores: The z-scores algorithm is based on the work of Brakel (Brakel, 2014). The standard deviation of the detector signal is calculated to define a confidence interval around the mean value. If the detector signal rises above the upper limit for a certain amount of time, this event is counted as a peak. At high concentrations, where more peaks are detected, the confidence interval would shift to a higher level. Small particle pulses cannot be detected anymore. To avoid this, an influence factor is introduced to reduce the impact of particle events on the calculation of the signal mean and standard deviation. A comprehensive introduction on the z-scores algorithm can be found online (Brakel, 2014). Brakel does also provide a good animation that shows the working principle of the algorithm. Further, a collection of code examples in the most common programming languages is available, which can be used for own implementations.

Vivó-Truyols: The algorithm is based on the work of Vivó-Truyols (Viv ó -Truyols et al., 2005). The derivates (0^{th}, 1st, and 2nd) of the detector signal are obtained with three Savitzky-Golay filters (Savitzky & Golay, 1964), which are implemented as FIR filters. The FIR coefficients depend on the selected polynomial degree, filter order, and derivative. Savitzky and Golay provided a Fortran code for the calculation of the coefficients (Savitzky & Golay, 1964). The optimal parameters for polynomial degree and filter order can be calculated by Durbin-Watson statistics as explained in (Viv ó -Truyols et al., 2005). Fig. 2 shows an example of a sampled detector signal and the corresponding derivates calculated with the FIR filter. The coefficients used for this example (filter order $N = 11$, polynomial degree $= 2$) are summarized in Table 2 (Appendix B).

If the second derivative falls below a predefined value for a certain amount of time, this event is counted as a particle. The work of Vivó-Truyols differentiates between moderate and strong coelution of the peaks. In the case of strong coeluted peaks, the third derivative has to be analyzed. This requires a high quality of the detector signal. For small particles the signal-to-noise ratio is lower because the pulse amplitudes are smaller. Thus, the algorithm has been implemented for the case of moderate coelution only.

Wavelet: The detector signal is convoluted with a Ricker wavelet. In contrast to the algorithms presented in (Du et al., 2006; Jiao et al., 2008; Zhao et al., 2019) the wavelet transformation is only calculated for a single scaling factor, which must be chosen so that the

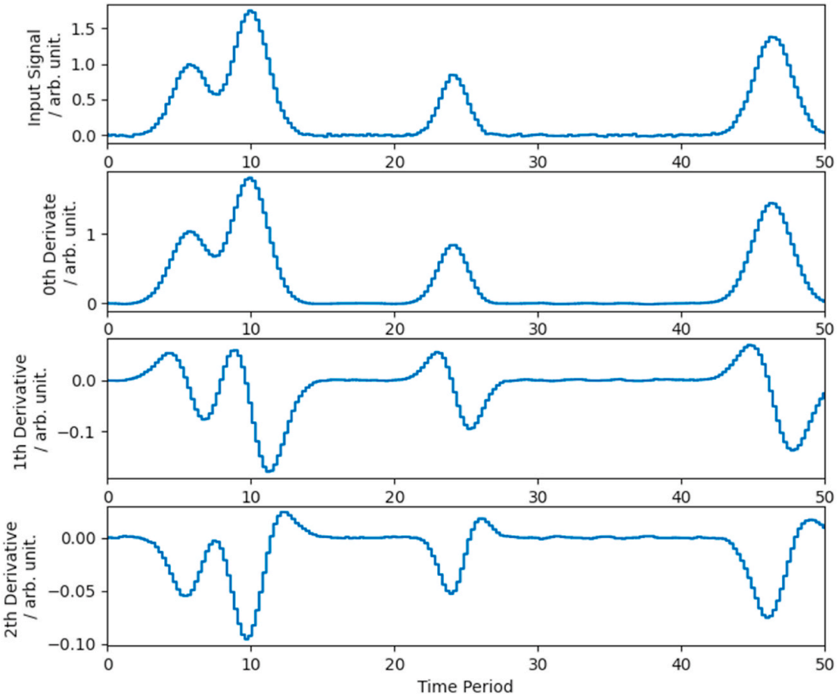

Fig. 2. Sampled detector input signal and derivates calculated with the Savitzky-Golay filter (filter order $N = 11$, polynomial degree $= 2$). The filter coefficients used in this example can be found in Table 2 (Appendix B). Each particle pulse generates a negative zone in the second derivative.

width of the kernel function does match with the width of the particle pulses. The particle pulses could be seen as maxima in the resulting signal. The wavelet signal is compared with a predefined threshold. If the wavelet signal is above this threshold for a certain amount of time, this event is counted as a particle.

Wavelet-Derivate: The detector signal is convoluted with a Ricker wavelet as described above. The particle pulses could be seen as a maxima in the resulting signal. The first derivative of the wavelet-signal is obtained with a Savitzky-Golay filter (Savitzky & Golay, 1964). The zeros of the derivative are counted as a particle. If the input signal does not contain particle pulses, the noise of the signal generates random zeros which would also be counted as particles. To avoid this, a second condition must be fulfilled: The input signal at the zero position has to be above a certain threshold value.

2.2. Measurement setup

Due to the fact that the quality and shape of the input signal can vary with the individual hardware setup, it must be ensured that the input signals for the different signal processing methods are the same. Otherwise, the overall system would be compared, not the algorithms for themselves. For this reason, the counting efficiency was determined with a measurement setup as schematically shown in Fig. 3.

A collision type (May 1973) aerosol generator (ATM 222, Topas GmbH, Dresden, Germany) was used to generate a Di-Ethyl-Hexyl-Sebacat (DEHS) aerosol. A differential electrical mobility classifier (Model 3080, TSI, Shoreview, USA) was used to generate aerosol particles with known size and distribution. A controlled blower (RFU 564, Topas GmbH, Dresden, Germany) was used to dilute the aerosol and decouple the fixed output flow of the generator from downstream devices. The particle concentration was adjusted with the air flow rate of the blower, without affecting the size distribution of the test aerosol. The evaluation was performed with a modified optical aerosol spectrometer (LAP 323, Topas GmbH, Dresden, Germany), which was equipped with an additional FPGA measurement board (Eclypse Z7, Digilent, Pullman, USA) and an analog front end (Zmod Scope 1410-125, Digilent, Pullman, USA). The analog-to-digital converter (ADC) inputs were directly connected to the detector output signal to ensure that analog and digital evaluation have to process the same input signal. Since the comparison of the number of particles counted by the different methods does not allow the determination of the counting efficiency curve, a scanning mobility particle sizer (SMPS, Model 3938L72, TSI, Shoreview, USA) was used as a reference to measure the actual concentration of the test aerosol. The system consists of another electrostatic classifier (Model 3082, TSI, Shoreview, USA) combined with a condensation particle counter (Model 3752, TSI, Shoreview, USA) and a 170 MBq ^{85}Kr neutralizer (Model 3077A, TSI, Shoreview, USA, 2010). With a known number concentration, the counting efficiency of the different methods were determined by the following equation (Equation (5)):

$$\eta = \frac{M_{counted}}{M_{actual}} = \frac{M_{counted}}{c \cdot \dot{V}_{LAP}} \qquad \text{Equation 5}$$

The SMPS and the aerosol spectrometer work both with a constant sample flow rate. Errors in the sample flow rate of both, SMPS and aerosol spectrometer cause a systematic error in the counting efficiency curve. The nominal sample flow rate of the used aerosol spectrometer was 0.1 l/min. The flow rate used for the calculation of the counting efficiency curves was adapted manually for each of the algorithms (ranging from 0.11 l/min to 0.115 l/min).

The measuring time of the aerosol spectrometer was set to 180 s for each data point. Before measuring the individual efficiency curves, the hyperparameters for the different algorithms need to be set to reasonable values. A poor choice of the parameters causes either a decreasing counting efficiency of the system, or an increased dark count rate (average rate of counted particles in clean air, due to detector noise). The optimization was done by hand to the best of the author's knowledge. All algorithms were adjusted to work as sensible as possible, under the condition that zero dark counts occur within a full measurement period.

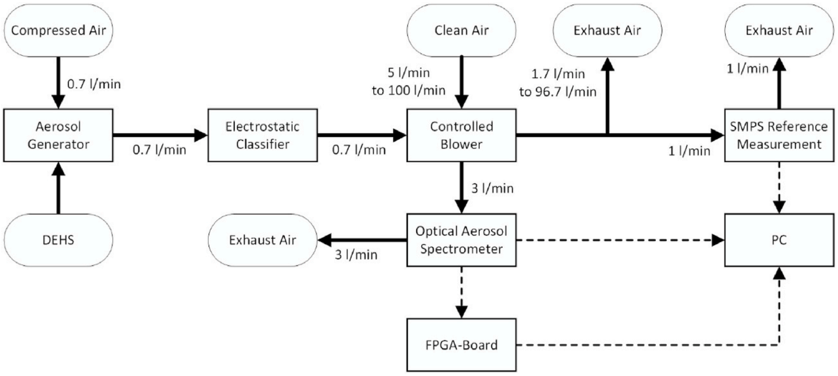

Fig. 3. Measurement setup: FPGA-Board and aerosol spectrometer receive the same detector signal. The actual concentration of the aerosol is determined by an SMPS reference measurement.

3. Results and discussion

In theory, the evaluation of the different detection algorithms could be done with any aerosol. Practically the reference aerosol has to meet certain criteria. For the proper calculation of the counting efficiency, all particles need to be in the measurement range of both, the aerosol spectrometer, and the SMPS system. The lower detection limit of the measurement setup with respect to particle size is approximately 150 nm. The pulse amplitudes of smaller particles are below the noise floor of the detector and cannot be detected. The maximum particle size of the SMPS system is 1 μm. Therefore an electrostatic classifier was used to define the size range of the test aerosol. The classification quality of an electrostatic classifier depends on the ratio between the aerosol and sheath flow rate Q_a/Q_{sh}. A high sheath flow rate yields to a narrow size distribution with secondary peaks caused by multiple charged particles. The actual size distribution of the reference aerosol does not significantly affect the results, because the main purpose of this study is to evaluate the counting efficiency with respect to number concentration. However, we decided to reduce the sheath flow rate until we received a broadly distributed aerosol with one major peak. Note that the reduced sheath flow rate does not reduce the amount of multiple charged particles, but blends the distribution of singly and doubly charged particles. Another requirement for the test aerosol is that its size distribution does not change with the concentration.

Fig. 4 shows the size distribution of the reference aerosol measured by the SMPS system at three different concentrations. As can be seen, the curves match each other. At low concentrations (e. g. 3700 cm^{-3}) only a small amount of particles is evaluated by the SMPS system, which leads to statistical fluctuations in the transformed density distribution. The cumulative distribution is less sensitive to this effect and shows that the size distribution of the aerosol is practically independent of the concentration. The median diameter of the aerosol is at about 350 nm. The proportion of particles smaller than 150 nm, and bigger than 1 μm is negligible in the test aerosol.

Fig. 5 shows the counting efficiency of the discussed algorithms plotted against concentration. The measurement results are plotted as points. According to Equation (2), an exponential model can be used for regression (Equation (6)):

$$\eta = m \cdot e^{-n \cdot c} \qquad \text{Equation 6}$$

Here, m describes the counting efficiency for the number concentration $c = 0\ \text{cm}^{-3}$, which is assumed to be 100%. The exponent n represents the product of the sample flow rate $\dot{V}$ and the detector dead time T_d. The dead time for the different algorithms can be obtained from any point of the exponential regression (Equation (7)):

$$T_d = \frac{\ln(\eta)}{-c \cdot \dot{V}} \qquad \text{Equation 7}$$

In Fig. 5 the regression curves are plotted as dotted lines for each series. The resulting detector dead times are shown in Table 1. For a direct comparison between the different algorithms, the scaled concentration can be used as a measure. Scaled concentration describes the extent to which the number concentration of the aerosol can be increased in comparison to a reference algorithm, with the same maximum coincidence error. E. g. a scaled concentration above 100% means that the algorithm is more efficient than the reference algorithm. The higher the scaled concentration, the better is the algorithm. In contrast, a scaled concentration below 100% implies that the algorithm is worse than the reference. The equation for the scaled concentration can be derived from Equation (2) and is given below (Equation (8)):

$$\mathit{Scaled\ Concentration} = \frac{c}{c_{analog}} = \frac{T_{d,\ analog}}{T_d} \qquad \text{Equation 8}$$

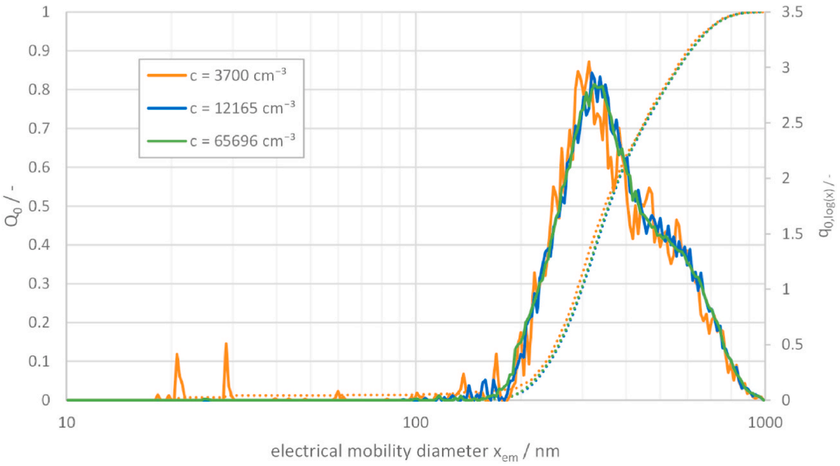

Fig. 4. SMPS-Reference measurement. Cumulative distribution and transformed distribution density of the DEHS test aerosol for different number concentrations. The dilution with the controlled blower does not affect the particle size distribution. Graphical representation according to ISO 9276–1:1998 (ISO 9276, 1998).

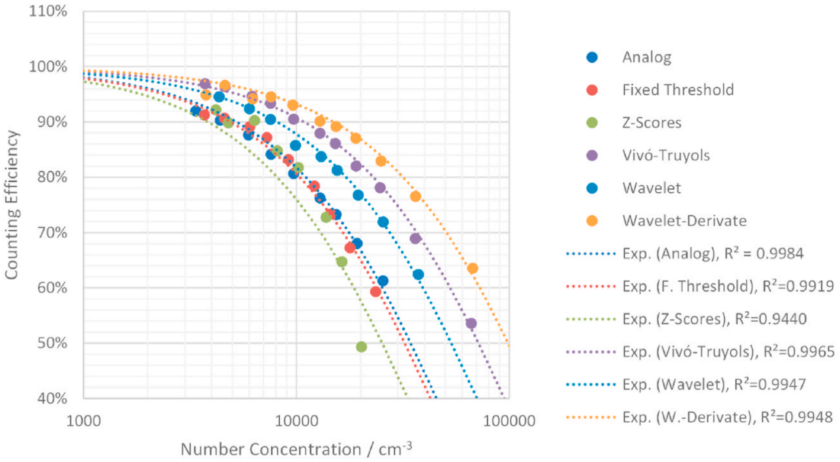

Fig. 5. Comparison of the different algorithms. Counting efficiency vs. number concentration. The dashed lines show the regression with the exponential model.

Table 1
Comparison between the algorithms. Scaled concentration is related to the analog evaluation of the optical aerosol spectrometer.

Algorithm	Dead Time/μs	Scaled Concentration/%
Analog (Reference)	10.73	100
Fixed Threshold	10.91	98
Z-Scores	14.95[a]	72
Vivó-Truyols	5.29	203
Wavelet	6.78	158
Wavelet-Derivate	3.67	292

[a] At high concentrations the exponential regression model is no longer valid, due to the threshold shift. For small concentrations the dead time is assumed to be comparable to the conventional threshold algorithms (approx. 10 μs).

In this work, the analog threshold-based peak detection of the aerosol spectrometer is used as a reference algorithm. The scaled concentrations for the different algorithms are given in Table 1.

The regression curves in Fig. 5 show the improvements in counting efficiency for aerosol spectrometers that can be achieved by digital signal processing techniques. The curve of the “Fixed Threshold” algorithm does match with the analog peak detection as expected. Therefore, a simple threshold-based algorithm does not improve the counting efficiency. The “Z-Scores” algorithm is even worse in this comparison, because of the shift of the confidence interval at higher concentrations. As a consequence, small particle

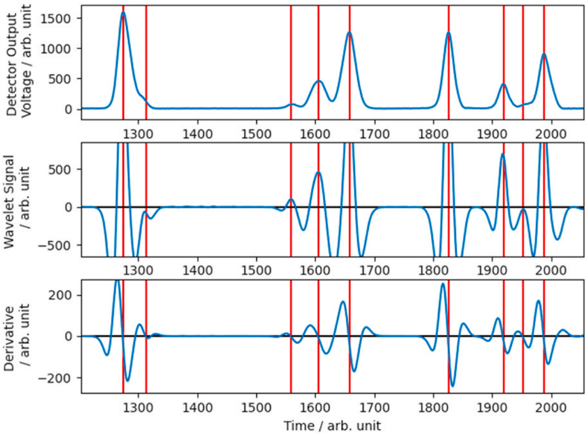

Fig. 6. Gaussian peak detection with the “Wavelet-Derivate”-algorithm. Signals from top to bottom: Detector input signal, wavelet-signal, and first derivate of the wavelet-signal. The vertical lines mark the detected peak positions.

pulses are excluded and the curve does not fit to the exponential regression model. It can be assumed that this effect can be minimized by better hyperparameter tuning. For small concentrations (below 10000 cm^{-3}) the counting efficiency is equal to other threshold-based algorithms. So the "Z-Scores" algorithm is not expected to be superior to the other algorithms. To further increase the counting efficiency, the shape of the particle pulses has to be analyzed.

The "Vivó-Truyols"-algorithm evaluates negative zones in the second derivative of the detector signal and is capable of detecting even strong coeluted particle pulses. The dead time of the algorithm is significantly shorter. This yields to an improved counting efficiency curve of the detector system. For a given maximum coincidence error the maximum aerosol concentration can be increased by a factor of 2.03. The threshold-based wavelet algorithm performs worse than Vivó-Truyols algorithm does. If two particle pulses with a different amplitude overlap each other, the resulting wavelet signal might stay below zero, although the second peak caused a local maxima on the signal. This effect can be seen in Fig. 6. The two small peaks at the positions 1310 AU and 1950 AU generate a local maximum on the wavelet signal, which is below zero at the peak positions. As a result, a threshold-based evaluation of the wavelet signal would not be able to detect those particle pulses.

This behavior can be improved by the evaluation of the first derivative of the wavelet-signal. The "Wavelet-Derivate" algorithm works based on this principle. This method can be used to reduce the dead time further. For a given maximum coincidence error the maximum aerosol concentration can be increased by a factor of 2.92.

As can be seen in Fig. 7 and Fig. 6, the "Wavelet-Derivate" algorithm is able to detect overlapping particle pulses. Thus, the coincidence error with respect to the amount of particles is smaller than in recent solutions. Optical aerosol spectrometers usually assign the particle pulses into different size classes. If the peaks of the individual particles are too close, the coincidences can also lead to an incorrect estimation of the peak amplitude (Fig. 7), which may cause a shift in the measured size distribution. Conventional algorithms (e. g. "Fixed-Threshold") cannot separate overlapping particle pulses. The classification is based on the maximum value of the detector signal. If two peaks with different amplitudes overlap each other, the decision is always in favor of the larger peak. This shifts the size distribution towards larger particles. In contrast, the "Wavelet-Derivate" algorithm can determine the position of the peaks. Thus, the relative error in the amplitude measurement remains small, even in the case of strong coelution. To illustrate this effect, we measured the size distribution of the test aerosol with the "Fixed Threshold" and "Wavelet-Derivative" algorithms. For this purpose, the aerosol spectrometer was calibrated with DEHS particles of different sizes. The SMPS system was used as a reference.

One important aerosol parameter is the median x_{50} of the size distribution. 50% of the counted particles are smaller than the median, while the other 50% are larger. At low concentrations, where no coincidences occur, the median measured with the aerosol spectrometer $x_{50,0}$ should match with the median of the SMPS system $x_{50,0,SMPS}$. Note that a systematic error can be caused by the calibration curve of the aerosol spectrometer. As mentioned before, the measured size distribution will shift towards larger particles, as the number concentration increases. The relative error between the measured and actual median can be used for comparison of the algorithms, and is determined as follows (Equation (9)):

$$Rel.\ Error = \frac{x_{50,0}}{x_{50,0,SMPS}} - 1 \qquad \text{Equation 9}$$

Fig. 8 shows the relative error of the median particle size for both, "Fixed Threshold", and "Wavelet-Derivate" algorithms. Below approx. 10000 cm^{-3} the relative errors for both algorithms are negligibly small. As expected, the median $x_{50,0}$ of the "Fixed Threshold" algorithm is noticeably shifted towards larger particles at higher concentrations. This error cannot be eliminated completely with the new algorithm, but it can be significantly minimized. The shift towards larger particles can be almost reduced to half, compared to recent solutions. In conclusion, the "Wavelet-Derivate" algorithm does not only minimize the coincidence error with respect to the amount of particles counted, but also with respect to the size distribution.

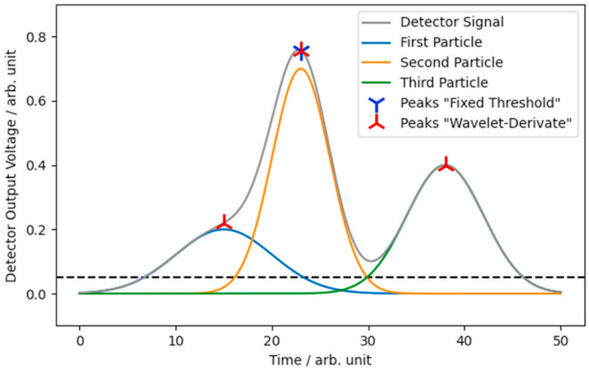

Fig. 7. Simulated detector signal of an aerosol spectrometer at high concentrations. The estimated peak apexes are shown for the "Fixed Threshold" and "Wavelet-Derivate" algorithms. The dashed line indicates the threshold level (0.05 AU) for the "Fixed Threshold" algorithm.

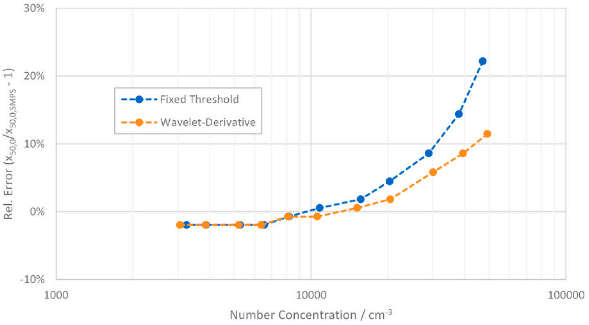

Fig. 8. Relative $x_{50,0}$ error of the size distribution against number concentration. The median of the acquired distribution with the SMPS system was used as a reference ($x_{50,0,SMPS} = 330$ nm).

4. Conclusions

Optical aerosol spectrometers are used to determine the size distribution and number concentration of aerosols. At high concentrations, the particle pulses tend to overlap each other. Therefore the concentration is underestimated, while the particle sizes tend to be overestimated. It is known that the coincidence error does not only depend on the number concentration of the aerosol, but also on the detector dead time. In general, a shorter dead time allows the aerosol spectrometer to measure at higher concentrations. In recent solutions, the detector signal is compared with a predefined threshold value. This algorithm is easy to implement but is not capable of detecting coeluted particle pulses, which results in a long dead time. To overcome this problem, several algorithms (Fixed Threshold, Z-Scores, Vivó-Truyols, Wavelet, Wavelet-Derivate) for Gaussian peak detection were implemented on an FPGA-evaluation board. The counting efficiency of each algorithm was measured with a real aerosol. As a result, the "Wavelet-Derivate" algorithm was able to reduce the detector dead time from 10.7 µs down to 3.7 µs. As shown in Fig. 6 even strong coeluted peaks can be found in the detector signal. This approach allows an increased maximum concentration for future aerosol spectrometers. By using digital signal processing methods aerosols with more than 2.9 times the number concentration can be quantified without increasing the coincidence error compared to current solutions. The advantage is that the algorithms can be implemented in existing solutions without redesigning the complex measuring cell. The presented method is not only limited to aerosol spectrometers but also can be extended to other instruments that need to evaluate Gaussian particle pulses (e. g. condensation particle counter).

The presented method mainly concerns the total amount of particles counted. Aerosol spectrometers assign the particle pulses to different size classes. If the Gaussian peaks overlap each other, the resulting amplitude is evaluated incorrectly, causing a shift of the actual size distribution towards larger particles. It was shown that the error can be significantly minimized, but not completely suppressed. An approach to overcome this might be to measure the time between the particle pulses. Only peaks with sufficient time differences are used for the size distribution. In other technical applications, the amplitudes of coeluting Gaussian peaks in stationary signals are reconstructed with inversion algorithms (Abramovitch, 2020; Li et al., 2018; Tong et al., 2016). The real-time implementation of such complex algorithms for the detector signal is quite challenging and could be the subject of further work.

Declaration of competing interest

The authors declare the following financial interests/personal relationships which may be considered as potential competing interests:

Lukas Oeser, Nakul Samala, Lars Hillemann, Andreas Rudolph, and Jens Lienig have no conflict of interest. Lukas Oeser, Nakul Samala, Lars Hillemann, and Andreas Rudolph are employees of the Topas GmbH, a company that develops, produces and markets aerosol technologies for research and industrial applications.

Appendix A

In the presented paper we show the advantages of wavelet-based peak detection algorithms for optical aerosol spectrometers. The following section should provide an overview, of how the wavelet transformation works, and how the wavelet transformation can be used practically.

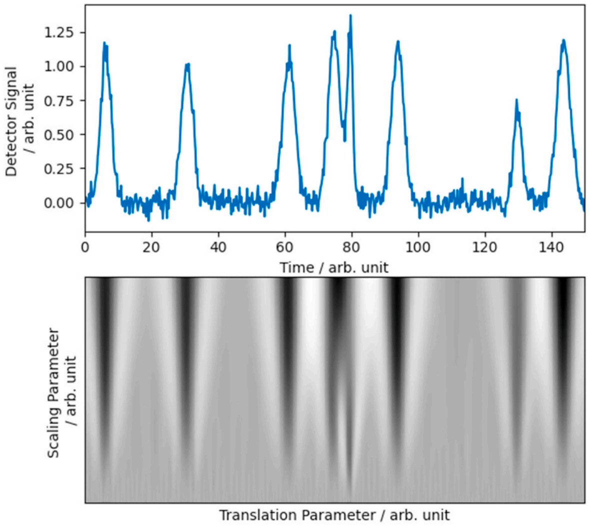

Fig. 9. Simulated noisy detector signal and corresponding wavelet transformation. Dark represents a higher value, and therefore a higher similarity between the kernel (ricker wavelet) and the detector signal

Fig. 9 shows a simulated detector signal of an optical aerosol spectrometer. As mentioned in the paper, the wavelet transformation can be interpreted as a convolution of a kernel function (e. g. ricker wavelet) with an input signal. The kernel function itself depends on two parameters. The scaling parameter a scales the kernel along the time-axis, while the translation parameter b shifts the kernel along the same axis. The value of the wavelet transformed signal at position $(a|b)$ expresses the similarity between the kernel, modified by the two parameters a and b, and the input signal.

In conclusion, the result of the wavelet transformation can be interpreted as a map with the coordinates translation and scaling parameter. The values of the wavelet-transformed signal would then correspond to the height profile of the map. As can be seen in Fig. 9, each particle pulse causes a local maxima, and therefore forms a ridgeline along the scaling parameter. If only one scaling parameter is used for the peak detection, this parameter has to be chosen wisely. The optimal value is a compromise between noise immunity and sensitivity to coeluted peaks. E. g. if the scaling factor is too big, the two peaks in Fig. 9 between 70 AU and 80 AU cannot be separated anymore. In contrast, a small scaling factor is able to separate the peaks, but is also more sensitive to noise.

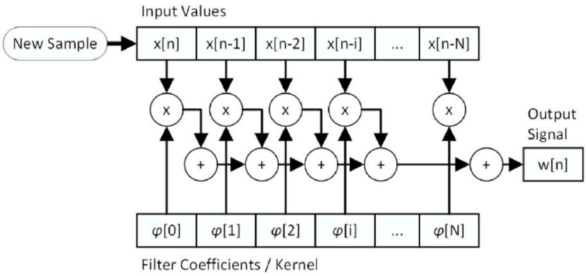

Fig. 10. FIR filter structure for the calculation of the wavelet transformed output signal. The filter can be implemented either in hard-, or software.

Practically, the calculation of the wavelet transformed signal can be done with a digital FIR filter. The FIR filter structure presented in Fig. 10 can be implemented either in hard-, or software. Although, a software-based solution is often easier to implement, the computing effort increases with the filter order. At higher sample rates a hardware-accelerated solution might become necessary. The calculation of the filter coefficients $\varphi[i]$, for a scaling factor a can be done with the following equation:

$$c[i] = \frac{1}{\sqrt{a}} \cdot \left(1 - \left(\frac{s-i}{a}\right)^2\right) \cdot e^{-\left(\frac{s-i}{a}\right)^2} \qquad \text{Equation 10}$$

The standard ricker wavelet function is symmetrical to the y-axis. As the indices of the FIR filter are usually assigned from 0 to N, a shift parameter s has to be used to center the kernel.

$$s = \frac{N-1}{2} \qquad \text{Equation 11}$$

For proper detection of the Gaussian-shaped particle pulses, the scaling parameter a must be selected depending on the pulse width. The right parameter choice can be found with try and error. A good starting point would be a value where the distance between the zeros of the ricker kernel matches to the width of the particle pulses (at e^{-1}-Level). According to the experience of the authors, the scaling parameter does not have to be chosen too precisely.

It should be mentioned that the maximum scaling factor is limited by the order of the FIR filter. The first and last filter coefficients should be close to zero. Otherwise, only a small part of the ricker kernel is used for convolution, which might result in an unexpected system behavior. E. g. for the presented FIR filter of the order 51 in Fig. 11, we would not recommend a scaling factor above 13.

Fig. 11 shows the computation of the wavelet-transformed signal for different scaling parameters. From top to bottom: Sampled input signal with a simulated Gaussian peak. The kernel coefficients for the different scaling parameters. The corresponding output signal of the FIR filter. Note that the response of the filter output has a delay, which depends on the filter size.

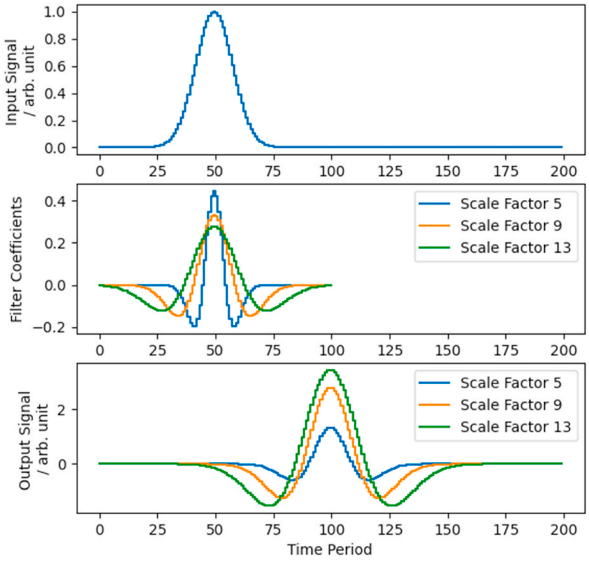

Fig. 11. Convolution of the input signal with different wavelet kernels using an FIR filter of the Order N = 51.

Appendix B

Table 2
FIR filter coefficients for the calculation of the 0^{th}, 1^{st}, and 2^{nd} derivative with the Savitzky-Golay filter of the order N = 11 and polynomial degree 2.

FIR coefficient	0^{th} Derivate	1st Derivate	2nd Derivate
φ [0]	−0.083916	−0.045455	0.034965
φ [1]	0.020979	−0.036364	0.013986
φ [2]	0.102564	−0.027273	−0.002331
φ [3]	0.160839	−0.018182	−0.013986
φ [4]	0.195804	−0.009091	−0.020979
φ [5]	0.207459	0.0	−0.02331
φ [6]	0.195804	0.009091	−0.020979
φ [7]	0.160839	0.018182	−0.013986
φ [8]	0.102564	0.027273	−0.002331
φ [9]	0.020979	0.036364	0.013986
φ [10]	−0.083916	0.045455	0.034965

References

Abramovitch, D. Y. (2020). Improved peak detection for mass spectrometry via augmented dominant peak removal. In *American control conference (ACC). 2020 American control conference* (pp. 5008–5015). ACC), 2020.

Brakel, J. P. G. van (2014). *Robust peak detection algorithm using z-scores*. Stack Overflow. Available at: https://stackoverflow.com/questions/22583391/peak-signal-detection-in-realtime-timeseries-data/22640362#22640362 (version: 2020-11-08).

Du, P., Kibbe, W. A., & Lin, S. M. (2006). Improved peak detection in mass spectrum by incorporating continuous wavelet transform-based pattern matching. *Bioinformatics, 22*(17), 2059–2065.

ISO 9276-1:1998-. *06 Representation of results of particle size analysis - Part 1: Graphical representation* (1998). Beuth Verlag GmbH.

Jiao, L., Gao, S., Zhang, F., & Li, H. (2008). Quantification of components in overlapping peaks from capillary electrophoresis by using continues wavelet transform method. *Talanta, 75*(4), 1061–1067.

Li, F., Gu, Z., Ge, L., Li, H., Tang, X., Lang, X., & Hu, B. (2019). Review of recent gamma spectrum unfolding algorithms and their application. *Results in Physics, 13*, Article 102211.

Liu, M., Dong, Z., Xin, G., Sun, Y., & Qu, R. (2018). An improved method based on a new wavelet transform for overlapped peak detection on spectrum obtained by portable Raman system. *Chemometrics and Intelligent Laboratory Systems, 182*, 1–8.

Li, L., Wu, Y., Dong, X., & Chi, B. (2018). Analysis of overlapping peaks of GA algorithms with early experience in integration. In *13th IEEE conference on industrial electronics and applications (ICIEA). 2018 13th IEEE conference on industrial electronics and applications* (pp. 90–94). ICIEA), 2018.

May, K. R. (1973). The collison nebulizer: Description, performance and application. *Journal of Aerosol Science, 4*(3), 235–243. https://doi.org/10.1016/0021-8502(73)90006-2

Mie, G. (1908). Beiträge zur Optik trüber Medien, speziell kolloidaler Metallösungen. *Ann. Phys., 330*(3), 377–445. https://doi.org/10.1002/andp.19083300302

Moelter, L., & Munzinger, F. (11 February 1998). Device and method for measuring particle fluxes in a fluid. *EP Patent EP0823626 (A2)*.

Raasch, J., & Umhauer, H. (1984). Der Koinzidenzfehler bei der Streulicht-Partikelgrössen-Zählanalyse. Fortschrittberichte der VDI-Zeitschriften. In *Reihe 3, Verfahrenstechnik* (p. 95). Düsseldorf: VDI-Verlag.

Sachweh, B. (1991). *Erweiterung des Meßbereiches eines Optischen Partikelzählers durch moderne*. digitale Signalverarbeitungstechniken.

Savitzky, A., & Golay, M. J. E. (1964). Smoothing and differentiation of data by simplified least squares procedures. *Analytical Chemistry, 36*(8), 1627–1639. https://doi.org/10.1021/ac60214a047

Tong, X., Zhang, Z., Zeng, F., Fu, C., Ma, P., Peng, Y., Lu, H., & Liang, Y. (2016). Recursive wavelet peak detection of analytical signals. *Chromatographia, 79*(19–20), 1247–1255.

VDI 3867 Blatt 4:2011-16. Measurement of particles in ambient air - determination of the particle number concentration and particle size distribution of aerosols - optical aerosol spectrometer. (2011). Beuth Verlag GmbH.

Vivó-Truyols, G., Torres-Lapasió, J. R., van Nederkassel, A. M., Vander Heyden, Y., & Massart, D. L. (2005). Automatic program for peak detection and deconvolution of multi-overlapped chromatographic signals part I: Peak detection. *Journal of Chromatography A, 1096*(1–2), 133–145.

Wee, A., Grayden, D. B., Zhu, Y., Petkovic-Duran, K., & Smith, D. (2008). A continuous wavelet transform algorithm for peak detection. *ELECTROPHORESIS, 29*(20), 4215–4225.

Zhao, X., Qin, Y., & Gianchandani, Y. B. (2019). Automatic peak integration and baseline correction for micro-scale gas chromatographs using continuous wavelet transform. In *IEEE SENSORS. 2019* (pp. 1–4). IEEE SENSORS, 2019.